Monolayer MoS$_2$: Trigonal warping, the Γ valley, and spin-orbit coupling effects

Andor Kormányos,[1,*] Viktor Zólyomi,[2] Neil D. Drummond,[2] Péter Rakyta,[3] Guido Burkard,[1] and Vladimir I. Fal'ko[2]

[1]*Department of Physics, University of Konstanz, D-78464 Konstanz, Germany*
[2]*Department of Physics, Lancaster University, Lancaster, LA1 4YB, United Kingdom*
[3]*Budapest University of Technology and Economics, Department of Theoretical Physics and Condensed Matter,
Research Group of the Hungarian Academy of Sciences, Budafoki út 8, H-1111 Budapest, Hungary*

We use a combined *ab initio* calculations and $\mathbf{k} \cdot \mathbf{p}$ theory based approach to derive a low-energy effective Hamiltonian for monolayer MoS$_2$ at the K point of the Brillouin zone. It captures the features which are present in first-principles calculations but not explained by the theory of Xiao *et al.* [Phys Rev Lett **108**, 196802 (2012)], namely the trigonal warping of the valence and conduction bands, the electron-hole symmetry breaking, and the spin splitting of the conduction band. We also consider other points in the Brillouin zone which might be important for transport properties. Our findings lead to a more quantitative understanding of the properties of this material in the ballistic limit.

I. INTRODUCTION

Transition metal dichalcogenides are emerging as promising new materials for applications in electronics and optoelectronics.[1] In particular, monolayer molybdenum disulfide (MoS$_2$) has recently received significant attention experimentally[2–11] as well as theoretically.[12–29] It may become the material of choice for field-effect transistors with high on-off ratio.[2] In addition, the strong spin-orbit coupling, the coupling between the spin and valley degrees of freedom,[12,14] and their effect on the exciton photoluminescence have sparked strong interest.[3–11] In light of the growing interest in this material, an accurate yet reasonably simple model that describes its band structure and electronic properties is highly desirable.

Following the important work in Refs. [30] and [31], Xiao *et al.*[12] have recently introduced a tight-binding model which assumes that at the K point of the Brillouin zone (BZ) it is sufficient to take into account the d_{z^2} (for the conduction band) and d_{xy}, $d_{x^2-y^2}$ (for the valence band) atomic orbitals of the Mo atoms. Neglecting the spin-orbit coupling (SOC), Xiao *et al.* found an effective Hamiltonian of the form $\hat{H}_0 = \hbar v_0 (\tau k_x \sigma_x + k_y \sigma_y) + \frac{\Delta}{2}\sigma_z$, where $\sigma_{x,y,z}$ denote Pauli matrices, Δ is the energy gap, v_0 plays the role of "Fermi velocity," and $\tau = 1 (-1)$ for valley K (K'). $\hat{H}_0$ describes massive Dirac particles, in other words, it is a monolayer graphene Hamiltonian with a staggered sublattice potential. While it seems to explain many experimental observations at least qualitatively,[5–7] certain limitations of this model can already be appreciated by looking at Figs. 1(b) and 1(c). The dispersion predicted by $\hat{H}_0$ is isotropic and possesses electron-hole symmetry regarding the valence and conduction bands. As one can see in Figs. 1(b) and 1(c), which show the results of first-principles calculations, except in the immediate vicinity of the K point, the dispersion is not isotropic: A trigonal warping (TW) of the isoenergy contours can clearly be seen. In comparison to monolayer graphene we note that its low-energy dispersion is isotropic on the energy scale of 1 eV, whereas in MoS$_2$ the TW is already observable at ≈ 0.08 eV below the

valence-band edge. Furthermore, *ab initio* calculations predict different effective masses for electrons and holes,[17,18,20] which obviously breaks the electron-hole symmetry. We also note that both our density functional (DFT) calculations and the computations of Refs. [17], [19], and [22] indicate that there is a relatively small (compared to the corresponding splitting in the valence band) but finite spin splitting of about 3–4 meV in the conduction band at the K point, which cannot be explained in the theoretical framework of Ref. [12]. Finally, as one can observe in Fig. 1(a) (see also the calculations of Refs. [17], [20], and [21]) the valence-band maximum (VBM) at the Γ point is actually very close in energy to the valence-band edge at the K point. While the exact value of the band maximum seems to depend on the particular computational method that is used [cf. Fig. 1(a) in Ref. [17] and Fig. 3 in Ref. [20]], it is clear that at finite temperatures in hole-doped samples states at both K and Γ points will participate in transport. (For the discussion of the importance of the additional satellite minima in the conduction band see Appendix C.) These observations call for a more exact model for the band structure of MoS$_2$.

Using our *ab initio* computations and the $\mathbf{k} \cdot \mathbf{p}$ theory[32] we show that the observed TW of the bands can be described by a four-band generalized bilayer-graphene-type Hamiltonian and the TW is understood as a consequence of the coupling of the valence band (VB) and conduction band (CB) to other (remote) bands. From the four-band model we derive an effective two-band model and obtain the parameters that enter the model from fitting to our DFT computations. SOC also plays an important role in the low-energy physics of MoS$_2$, but the SOC Hamiltonian cannot be obtained from results on bilayer graphene.[33,34] We find that a consistent description requires a seven-band model (or 14-band model, including the spin) at the K point and a six-band model at the Γ point. We derive an effective low-energy Hamiltonian which takes into account the effects of the SOC, including the spin splitting of the CB, which, to our knowledge, has not been considered in detail before. We also discuss how the effective mass and various other parameters of the model depend on the SOC.
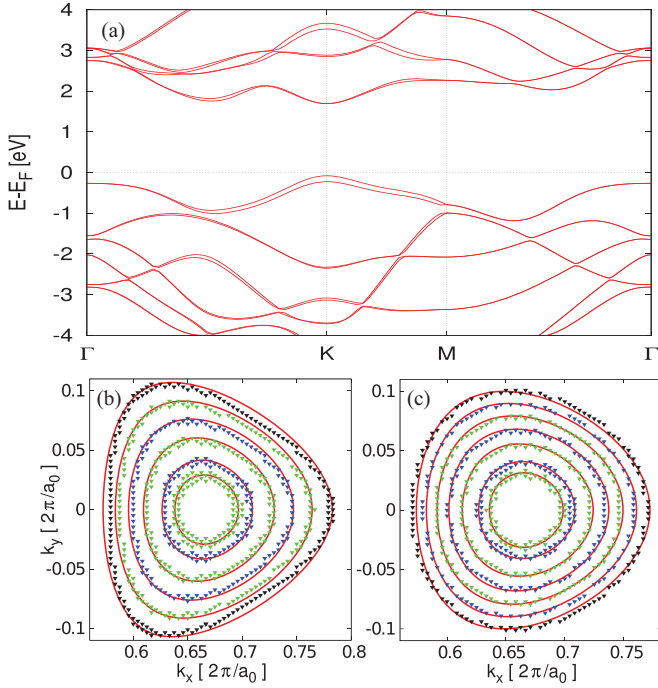
FIG. 1. (Color online) (a) Spin-resolved band structure of MoS$_2$ from DFT LSDA calculations. (b) Contour plot showing the isoenergy contours of the valence band (for zero SOC) from DFT calculations at the K point of the BZ (symbols) and as obtained from Eq. (2) (solid lines). (c) The same as in (b) for the conduction band. a_0 is the lattice constant. The energy difference between the two innermost contours is 0.02 eV, between every other contours is 0.04 eV.

II. EFFECTIVE HAMILTONIAN

We start with the derivation of the spinless effective Hamiltonian, i.e., we neglect the SOC. This is already sufficient to explain the TW of the isoenergy contours. We make repeated use of various symmetries of the crystal structure, the two most important of which for our purposes are the rotational symmetry by $2\pi/3$ around an axis perpendicular to the plane of MoS$_2$ (we denote it by C_3) and the horizontal mirror plane σ_h. (For the full point group symmetry see Appendix A.) The derivation of the effective Hamiltonian relies on our DFT calculations, which, in addition to the band structure, provide us with the projection of the DFT wave functions onto atomic orbitals at high symmetry points of the BZ. This helps us to identify the symmetries of the bands, which is necessary to obtain the general form of the effective Hamiltonian. As an example we consider the (topmost) valence and the (lowest) conduction bands at the K point of the BZ. Similarly to Refs. 12 and 20–22, we find that here the VB is predominantly composed of the $d_{x^2-y^2}$ and d_{xy} atomic orbitals centered on the Mo atoms, which are symmetric with respect to σ_h. Since the VB is nondegenerate at the Γ point, compatibility relations require that at the K point it transforms as the A' representation of the group C_{3h}, which is the small group of the wave vector at K. We denote the wave function of the VB by $|\Psi_{A'}^v\rangle$, and hereafter we use the notation $|\Psi_\mu^b\rangle$ for the wave functions of

various bands, where b denotes the band and μ the pertinent irreducible representation (irrep). The CB is predominantly composed of d_{z^2} orbitals of the Mo atoms,[12,20–22] which means that the CB wave function $|\Psi_{E_1'}^c\rangle$ is also symmetric with respect to σ_h and transforms as the E_1' irrep of C_{3h}. Similar considerations allow us to obtain the symmetries of all bands at the K point, even when different orbitals from different atoms are admixed (see Appendix A). In a minimal model that captures TW, in addition to the VB and the CB, there are two other important bands, both of which are even with respect to σ_h: the second one above the CB, which we denote by CB+2 and whose wave function is $|\Psi_{E_2'}^{c+2}\rangle$ and the third one below the valence band (VB-3) with wave function $|\Psi_{E_2'}^{v-3}\rangle$. The other bands between the VB-3 and CB+2 are antisymmetric with respect to the mirror plane of MoS$_2$ and therefore they do not couple to the VB and the CB. In $\mathbf{k} \cdot \mathbf{p}$ theory the Hamiltonian $\mathcal{H}_{\mathbf{k}\cdot\mathbf{p}} = \frac{\hbar}{m_e}\mathbf{k} \cdot \hat{\mathbf{p}}$ is considered a perturbation (m_e is the bare electron mass) and one uses first-order perturbation theory in the basis of $\{|\Psi_{A'}^v\rangle, |\Psi_{E_1'}^c\rangle, |\Psi_{E_2'}^{v-3}\rangle, |\Psi_{E_2'}^{c+2}\rangle\}$. Using the notation $\mathbf{k} = \mathbf{q} + \mathbf{K}$, the perturbation can be rewritten as $\mathcal{H}_{\mathbf{k}\cdot\mathbf{p}} = \frac{1}{2}\frac{\hbar}{m_e}(q_+\hat{p}_- + q_-\hat{p}_+) = \mathcal{H}_{\mathbf{k}\cdot\mathbf{p}}^- + \mathcal{H}_{\mathbf{k}\cdot\mathbf{p}}^+$, where the operators $\hat{p}_\pm$ are defined as $\hat{p}_\pm = \hat{p}_x \pm i\hat{p}_y$ and similarly $q_\pm = q_x \pm iq_y$. The matrix elements of $\mathcal{H}_{\mathbf{k}\cdot\mathbf{p}}$ are constrained by the symmetries of the system. For example, considering the rotation C_3, the relation $\langle\Psi_{A'}^v|\hat{p}_+|\Psi_{E_2'}^{c+2}\rangle = \langle\Psi_{A'}^v|C_3^\dagger C_3 \hat{p}_+ C_3^\dagger C_3|\Psi_{E_2'}^{c+2}\rangle$ should hold. Since $\langle\Psi_{A'}^v|C_3^\dagger = \langle\Psi_{A'}^v|$, $C_3\hat{p}_\pm C_3^\dagger = e^{\mp i2\pi/3}\hat{p}_\pm$, and $C_3|\Psi_{E_2'}^{c+2}\rangle = e^{-i2\pi/3}|\Psi_{E_2'}^{c+2}\rangle$ one obtains that $\langle\Psi_{A'}^v|\mathcal{H}_{\mathbf{k}\cdot\mathbf{p}}^+|\Psi_{E_2'}^{c+2}\rangle = e^{-i4\pi/3}\langle\Psi_{A'}^v|\mathcal{H}_{\mathbf{k}\cdot\mathbf{p}}^+|\Psi_{E_2'}^{c+2}\rangle$, which means that this matrix element must vanish. By contrast, $\langle\Psi_{A'}^v|\hat{p}_-|\Psi_{E_2'}^{c+2}\rangle = \gamma_4$ is finite and one can prove that it is a real number. Similar considerations can be used to calculate all matrix elements. Finally, in the basis of $\{|\Psi_{A'}^v\rangle, |\Psi_{E_1'}^c\rangle, |\Psi_{E_2'}^{v-3}\rangle, |\Psi_{E_2'}^{c+2}\rangle\}$ the $\mathbf{k} \cdot \mathbf{p}$ Hamiltonian at the K point is given by

$$H_{\mathbf{kp}} = \begin{pmatrix} \varepsilon_v & \gamma_3 q_- & \gamma_2 q_+ & \gamma_4 q_+ \\ \gamma_3 q_+ & \varepsilon_c & \gamma_5 q_- & \gamma_6 q_- \\ \gamma_2 q_- & \gamma_5 q_+ & \varepsilon_{v-3} & 0 \\ \gamma_4 q_- & \gamma_6 q_+ & 0 & \varepsilon_{c+2} \end{pmatrix}, \quad (1)$$

where γ_i are the matrix elements of $\mathcal{H}_{\mathbf{k}\cdot\mathbf{p}}$ in the above mentioned basis and $\varepsilon_v, \varepsilon_c, \varepsilon_{v-3}, \varepsilon_{c+2}$ are band-edge energies. The matrix element between $|\Psi_{E_2'}^{v-3}\rangle$ and $|\Psi_{E_2'}^{c+2}\rangle$ vanishes due to symmetry. We note in passing that the Hamiltonian (1) can be considered a generalized bilayer graphene (BLG) Hamiltonian.[35] This can be seen by rotating the well known bilayer graphene Hamiltonian into a basis where the basis functions transform according to the irreps of the small group of BLG (see Appendix B). To obtain the $\mathbf{k} \cdot \mathbf{p}$ Hamiltonian at the K' point it proves to be useful to re-define $q_\pm$ as $q_\pm = q_x \pm i\tau q_y$, where $\tau = 1(-1)$ for the K (K') point. As in the case of BLG, it is convenient to derive a low-energy effective Hamiltonian from (1), which does not contain the contribution of the bands far from the Fermi energy. Using the

Löwdin partitioning[36] we find

$$H_{\text{eff}} = H_0 + H_{\text{as}} + H_{3w} + H_{\text{cub}}, \quad (2a)$$

$$H_0 + H_{\text{as}} = \begin{pmatrix} \varepsilon_v & \tau \, \gamma_3 q_- \\ \tau \, \gamma_3 \, q_+ & \varepsilon_c \end{pmatrix} + \begin{pmatrix} \alpha q^2 & 0 \\ 0 & \beta q^2 \end{pmatrix}, \quad (2b)$$

$$H_{3w} = \kappa \begin{pmatrix} 0 & (q_+)^2 \\ (q_-)^2 & 0 \end{pmatrix}, \quad (2c)$$

$$H_{\text{cub}} = -\tau \, \frac{\eta}{2} q^2 \begin{pmatrix} 0 & q_- \\ q_+ & 0 \end{pmatrix}, \quad (2d)$$

where the parameters α, β, κ, and η can be expressed in terms of γ_i as defined in Eq. (1) and the band-edge energies. The parameters α and β describe the breaking of the electron-hole symmetry that is apparent comparing Figs. 1(b) and 1(c), whereas κ is responsible for the TW of the energy contours. The cubic term H_{cub} is important to achieve a quantitative fit to the VB away from the K point. We note that symmetries allow for another, diagonal Hamiltonian which is $\sim q^3$, but its effect has been found to be negligible.

We used the VASP code[37] and the local density approximation (LDA) of DFT to calculate[38] the band structure and isoenergy contours shown in Fig. 1. To compare our $\mathbf{k} \cdot \mathbf{p}$ theory with the DFT calculations one has to determine the matrix elements γ_i. These matrix elements, in principle, can also be calculated from DFT.[39] We found however that the isoenergy lines calculated with parameters γ_i^{DFT} obtained from the numerical evaluation of $\langle \Psi_\mu^b | \hat{p}_\pm | \Psi_{\mu'}^{b'} \rangle$ using Kohn-Sham orbitals[40] give a satisfactory agreement with DFT band structure only in the close vicinity of the K point. Therefore we used these γ_i^{DFT} values as a starting point for a fitting procedure, whereby we fitted the eigenvalues of the Hamiltonian (2) [given in terms of $\gamma_3, \alpha, \beta, \kappa, \eta$, and the band-edge energies ε_v, and ε_c] along the ΓKM line to the CB and VB obtained from the DFT calculations. The fit involved a range of $\approx 0.1 \times \frac{2\pi}{a_0}$ in the Γ and M directions. From the fitting we found the parameters $\gamma_3 = 3.82 \text{ eV Å}, \alpha = 1.72 \text{ eV Å}^2, \beta = -0.13 \text{ eV Å}^2$, $\kappa = -1.02 \text{ eV Å}^2$, and $\eta = 8.52 \text{ eV Å}^3$. The isoenergy contours calculated using these parameters [the solid lines in Figs. 1(b) and 1(c)] capture well the TW of the band dispersion (cf. the results of the DFT computations given by symbols), which is more pronounced in the VB than in the CB. The agreement between the DFT results and the predictions based on (2) is very good up to energies 0.16 eV below the VB maximum and above the CB minimum; for other energies the agreement is qualitative. The effective masses (along the ΓKM line) that can be inferred from these parameters are $m_{\text{eff}}^v \approx -0.62 m_e$ for the VB and $m_{\text{eff}}^c \approx 0.48 m_e$ for the CB, which are in good agreement with the results of other DFT LDA calculations.[16,23] (For a similar set of parameters based on band structure calculations using the HSE06 hybrid functional, see Appendix D). Interestingly, we have checked by numerical calculations that although the TW is quite strong in the VB, its effect on the Landau levels is actually very small, and they can be calculated by neglecting H_{3w} in Eq. (2). Nevertheless, H_{3w} and H_{cub} should affect the Berry curvature and hence various Hall conductivities.[12,24]

An important feature of the band structure of MoS$_2$, which has received little attention so far, is that the top of the valence band at the Γ point is very close in energy to the VBM at the K point[17,20,21]; see also Fig. 1(a). This means that for the VB transport properties the states close to the Γ point can also be important. The Hamiltonian of this "Γ valley" can also be derived using the $\mathbf{k} \cdot \mathbf{p}$ theory, along similar lines to the case of the K point. Note, however, that the group of the wave vector at the Γ point is D_{3h}. Our DFT calculations show that here the VB is mainly composed of the d_{z^2} and s orbitals of the Mo atoms and the p_z orbitals of the S atoms, which means that it belongs to the A_1' irrep of D_{3h}. The VB is coupled to the VB-3 and CB $+1$ bands which are doubly degenerate at the Γ point. There is no coupling between the VB and the CB at the Γ point: Due to band crossings along the Γ-K line the CB becomes antisymmetric with respect to σ_h. Upon performing the Löwdin partitioning we find that the dispersion is isotropic and can be well described by $\mathcal{H}_\Gamma = \frac{\hbar^2 k^2}{2m_{\text{eff}}^\Gamma}$, where the effective mass $m_{\text{eff}}^\Gamma = -3.65 m_e$ is found by fitting the band structure, which is in good agreement with Ref. 23. The importance and role of the Γ point in the transport properties of the VB would require further experimental work. We expect that in disordered samples due to their large effective mass and hence low mobility the contribution of these states to the transport is small, but they may be important in ballistic samples and in quantum-Hall measurements.

III. SPIN-ORBIT COUPLING

The description of the system becomes more complicated if one takes into account the SOC as well. In the atomic approximation the SOC is given by the Hamiltonian

$$\mathcal{H}_{\text{so}}^{\text{at}} = \frac{\hbar}{4m_e^2 c^2} \frac{1}{r} \frac{dV(r)}{dr} \mathbf{L} \cdot \mathbf{S}. \quad (3)$$

Here $V(r)$ is the spherically symmetric atomic potential, $\mathbf{L}$ is the angular momentum operator, and $\mathbf{S} = (S_x, S_y, S_z)$ is a vector of spin Pauli matrices S_x, S_y (with eigenvalues ± 1). Note that $\mathbf{L} \cdot \mathbf{S} = L_z S_z + L_+ S_- + L_- S_+$, where $L_\pm = L_x \pm i L_y$ and $S_\pm = \frac{1}{2}(S_x \pm i S_y)$. Let us introduce the spinful symmetry basis functions by $|\Psi_\mu^b, s\rangle = |\Psi_\mu^b\rangle \otimes |s\rangle$, where $s = \{\uparrow, \downarrow\}$ denotes the spin degree of freedom, and consider first the K point of the BZ. Since $L_\pm$ transforms as the E'' irrep of C_{3h}, there can be nonvanishing matrix elements of $\mathcal{H}_{\text{so}}^{\text{at}}$ between states that are even/odd with respect to σ_h. Therefore we considered a seven-band model (without spin) which contains every band between VB-3 and CB $+2$, i.e., we consider the basis $\{|\Psi_{E_2'}^{v-3}, s\rangle, |\Psi_{E_1''}^{v-2}, s\rangle, |\Psi_{E_2'}^{v-1}, s\rangle, |\Psi_{A_1'}^v, s\rangle, |\Psi_{E_1'}^c, s\rangle, |\Psi_{A_1''}^{c+1}, s\rangle, |\Psi_{E_1'}^{c+2}, s\rangle\}$. The symmetries σ_h and C_3 of the system here also help us to find the nonzero matrix elements of $\mathcal{H}_{\text{so}}^{\text{at}}$. For example, one can make use of the fact that $C_3 L_\pm C_3^\dagger = e^{\mp i 2\pi/3} L_\pm$ and therefore show that $\langle s, \Psi_{A_1'}^v | L_- S_+ | \Psi_{E_2''}^{v-1}, s\rangle = \Delta_{(v, v-1)} S_+$, where $\Delta_{(v, v-1)}$ is a constant, whereas $\langle s, \Psi_{A_1'}^v | L_+ S_- | \Psi_{E_2''}^{v-1}, s\rangle = \langle s, \Psi_{A_1'}^v | L_z S_z | \Psi_{E_2''}^{v-1}, s\rangle = 0$. By calculating the matrix $H_{\text{so}}^{\text{at}}$ in the above mentioned basis and diagonalizing the Hamiltonian $H_d + H_{\text{so}}^{\text{at}}$, where H_d is a diagonal matrix containing the band-edge energies, one obtains the eigenstates $|\Psi_{\mu, \mu'}^b, s\rangle$,

which in general turn out to be linear combinations of a symmetric $|\Psi^b_\mu, s\rangle$ and an antisymmetric $|\Psi^{b'}_{\mu'}, s\rangle$ wave function with different weights. In our notation the new eigenstates $|\Psi^b_{\mu,\mu'}, s\rangle$ inherit the band index b and spin index s from the state whose weight is larger in the linear combination that makes up $|\Psi^b_{\mu,\mu'}, s\rangle$. This assignment of the band index and spin quantum number is possible because the typical energy scale of the SOC (the upper limit of which is the splitting of the valence band ≈ 145 meV, see below) is significantly smaller than the typical band separation, i.e., the bands are not strongly hybridized by the SOC. The diagonalization of the Hamiltonian can be done analytically in the approximation that couplings of up to next-nearest-neighbor bands are kept and more remote couplings, e.g., between $|\Psi^{v-3}_{E'_2}, s\rangle$ and $|\Psi^{c+1}_{A''}, s\rangle$, are neglected. All eigenstates are nondegenerate, as expected, since the double group of C_{3h} has only one-dimensional representations. With the new eigenstates $|\Psi^b_{\mu,\mu'}, s\rangle$ one can repeat the $\mathbf{k} \cdot \mathbf{p}$ calculation, and since $|\Psi^b_{\mu,\mu'}, s\rangle$ is an admixture of symmetric and antisymmetric states, there will be more nonzero matrix elements of the $\mathcal{H}_{\mathbf{k}\cdot\mathbf{p}}$ Hamiltonian than there were in the case of zero spin-orbit coupling; see Eq. (1). Finally, using the Löwdin partitioning we can derive an effective low-energy Hamiltonian for the spinful valence and conduction bands. Since the calculations are quite lengthy, we only give the most important results here and concentrate on the zero-magnetic field case. The Landau-level problem in the presence of SOC and the related question of the effective g factor of monolayer MoS$_2$ will be discussed elsewhere.

We will work in the basis of $\{|\Psi^v_{A', E''_2}, \uparrow\rangle, |\Psi^v_{A', E''_1}, \downarrow\rangle, |\Psi^c_{E'_2, E''_1}, \uparrow\rangle, |\Psi^c_{E'_2, A''}, \downarrow\rangle\}$ and start with the diagonal and $\mathbf{q}$ independent part of the SOC Hamiltonian, i.e., we consider the SOC dependence of the band-edge energies. According to our $\mathbf{k} \cdot \mathbf{p}$ calculations, the spin splitting in the VB and the CB can be described by the Hamiltonians

$$H^{\mathrm{so}}_{vb} = -\tau \Delta^v_1 S_z + \frac{\Delta^v_2}{2}(\mathbb{1} + \tau S_z), \tag{4a}$$

$$H^{\mathrm{so}}_{cb} = \frac{|\Delta^c|^2}{2}\left[\frac{\mathbb{1} - \tau S_z}{\varepsilon_c - \varepsilon_{v-1}} - \frac{\mathbb{1} + \tau S_z}{\varepsilon_{c+1} - \varepsilon_c}\right]. \tag{4b}$$

The term $-\tau \Delta^v_1 S_z$ was first obtained in Ref. 12, whereas the second term of H^{so}_{vb}, which is expected to be much smaller, comes from the coupling of spin-up (spin-down) band of VB to VB-1 at the K (K') point. [The coupling of the spin-down (spin-up) band of the VB to other bands is much weaker.] Our DFT calculations give a spin-orbit gap of $2\Delta^v_1 - \Delta^v_2 \approx 146$ meV in the VB. The spin splitting of the CB, given by Eq. (4b), although noted in that it is nonzero in the numerical calculations of Refs. 17, 19, and 22, has not yet been discussed in detail in the literature.[42] It originates from the SOC of the CB to the VB-1 and CB+1 bands and is a consequence of the hitherto neglected off-diagonal SOC terms, related to the $\sim L_- S_+ + L_+ S_-$ part of $\mathcal{H}^{\mathrm{at}}_{\mathrm{so}}$. Our results therefore show that the spin-valley coupling is present not only in the VB[12] but also in the CB. Our DFT computations give a spin splitting of $|\Delta^c|^2[\frac{1}{\varepsilon_c - \varepsilon_{v-1}} + \frac{1}{\varepsilon_{c+1} - \varepsilon_c}] \approx 3$ meV. Although this is a small effect compared to the spin splitting in the VB, spin splittings of similar magnitude have recently been measured in, e.g., carbon

nanotube quantum dots.[43] We note that further, $\mathbf{q}$-dependent terms beyond those shown in Eq. (4) can also be derived, which may in some cases be important. However, our DFT calculations suggest that the $\mathbf{q}$ dependence of the spin splitting in the vicinity of the K point is not strong; therefore we do not consider those terms here.

Regarding the effect of SOC on the $\mathbf{q}$-dependent terms in Eq. (2), we find that bands with different spin indices, e.g., $\{|\Psi^v_{A', E''_2}, \uparrow\rangle$ and $|\Psi^v_{A', E''_1}, \downarrow\rangle$ or $|\Psi^c_{E'_2, A''}, \downarrow\rangle\}$ do not couple to each other. After folding down the full seven-band $\mathbf{k} \cdot \mathbf{p}$ Hamiltonian, in the basis of $\{|\Psi^v_{A', E''_2}, \uparrow\rangle, |\Psi^c_{E'_2, E''_1}, \uparrow\rangle\}$, and $\{|\Psi^v_{A', E''_1}, \downarrow\rangle, |\Psi^c_{E'_2, A''}, \downarrow\rangle\}$ the effective Hamiltonian is still of the form of Eq. (2), but in general with different parameters $\gamma_3^{\uparrow(\downarrow)}, \alpha^{\uparrow(\downarrow)}, \beta^{\uparrow(\downarrow)}, \kappa^{\uparrow(\downarrow)}$, and $\eta^{\uparrow(\downarrow)}$ for the spin-up (spin-down) bands. By fitting our SOC-resolved DFT calculations we find that γ_3 and β, hence m^c_{eff}, are basically not affected by the SOC. The effective masses in the VB are slightly renormalized by the SOC, leading to $m^{v,\uparrow}_{\mathrm{eff}} \approx 0.65 m_e$ and $m^{v,\downarrow}_{\mathrm{eff}} \approx 0.58 m_e$, i.e., a difference of roughly 5%–6% with respect to the zero SOC case.

Finally, we briefly discuss the effect of SOC on the states at the Γ point of the BZ. In contrast to the K point, here the valence band remains degenerate even if we take into account SOC (see Fig. 1). This can be understood from general group theoretical arguments: The pertaining double group has two-dimensional, hence degenerate representations. The dispersion for each spin can be described by a parabolic dependence on $\mathbf{k}$ and we find that the effective mass is basically unchanged with respect to the zero SOC case.

IV. CONCLUSIONS

We have derived a low-energy effective Hamiltonian for monolayer MoS$_2$ at the K point of the BZ, which takes into account effects that are present in first-principles calculations but have not hitherto been discussed. Our theory is valid at low densities and for perfectly flat monolayer MoS$_2$ crystals. The TW and spin splitting of the bands should be readily observable by spin and angle resolved photoemission spectroscopy. We have also considered the states at the Γ point of the BZ, which can be important for transport properties of hole-doped samples as well as for various scattering and relaxation processes,[25,28,29] because scattering from the K to the Γ point does not require a simultaneous valley and spin flip.

Note added. During the preparation of this manuscript a related preprint has appeared,[44] where some of the results that we present here have also been obtained.

APPENDIX A: CHARACTER TABLES AND BASIS FUNCTIONS

In Fig. 2 we show a top view of the monolayer MoS$_2$ lattice. The pertinent point groups to understand the band structure of
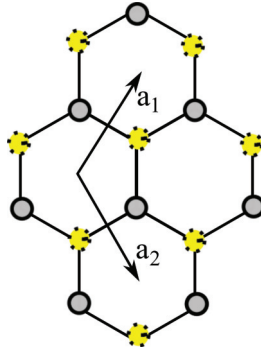
FIG. 2. (Color online) Top view of the MoS$_2$ lattice. Mo atoms are indicated by gray (solid line) circles, S atoms by yellow (dotted line) circles. The lattice vectors $\mathbf{a}_1 = \frac{a_0}{2}(1,\sqrt{3})$ and $\mathbf{a}_2 = \frac{a_0}{2}(1,-\sqrt{3})$ are also shown ($a_0 = 3.129$ Å is the lattice constant).

monolayer MoS$_2$ are D_{3h} and C_{3h}. The former is the group of the wave vector at the Γ point, the latter at the K point of the Brillouin zone (BZ). The symmetry operations that generate these groups are threefold rotation C_3 around an axis perpendicular to the plane of MoS$_2$, a horizontal mirror plane σ_h perpendicular to the threefold axis, and in the case of D_{3h}, three twofold rotation axis C_2' that lie in the horizontal mirror plane.

By projecting the plane-wave basis used in our DFT computations onto atomic orbitals one can obtain the decomposition of each band in terms of atomic orbitals Φ_ν^η, where $\eta = \{$Mo,S1,S2$\}$ denotes whether the given orbital is centered on molybdenum (Mo) or on one of the sulfur (S1, S2) atoms in the unit cell, and the lower index $\nu = \{s, p_x, p_y, p_z, d_{z^2}, d_{xy}, d_{xz}, d_{xy}, d_{x^2-y^2}\}$ indicates the type of orbital. To take into account the threefold rotational symmetry of the system, one should use linear combinations of these orbitals to form the rotating orbitals Y_l^m, which are proportional to spherical harmonics. We then consider the transformation properties of the Bloch wave functions formed with the rotating orbitals:

$$\left|\Psi_{l,m}^\eta(\mathbf{k},\mathbf{r})\right\rangle = \frac{1}{\sqrt{N}} \sum_n e^{i\mathbf{k}\cdot(\mathbf{R}_n+\mathbf{t}_\eta)} Y_l^m(\mathbf{r} - [\mathbf{R}_n + \mathbf{t}_\eta]).$$

Here the summation runs over all lattice vectors $\mathbf{R}_n$ and $\mathbf{t}_{\text{Mo}} = \frac{a_0}{2}(1,-\frac{1}{\sqrt{3}})^T$, $\mathbf{t}_{\text{S1}} = \mathbf{t}_{\text{S2}} = \frac{a_0}{2}(1,\frac{1}{\sqrt{3}})^T$ give the position of the Mo and S atoms in the (two-dimensional) unit cell with $a_0 = 3.129$ Å being the lattice constant (see also Fig. 2) and $\mathbf{k}$ is measured from the Γ point of the BZ. We then identify the irreducible representations (irreps) according to which $\left|\Psi_{l,m}^\eta(\mathbf{k},\mathbf{r})\right\rangle$ transform at the high symmetry points Γ and K of the BZ. Since hybridization between different orbitals will preserve the symmetry properties, the analysis of the bands in terms of atomic orbitals, together with band compatibility relations, gives us the irreps that can be assigned to each band.

As an example we consider the valence band (VB) at the K point. Here the VB is predominantly composed of the $d_{x^2-y^2}$ and d_{xy} atomic orbitals centered on the Mo atoms, which are symmetric with respect to σ_h. The two Bloch functions that can be formed from these orbitals and which reflects the threefold rotational symmetry are $\left|\Psi_{2,\pm 2}^{\text{Mo}}(\mathbf{k})\right\rangle = \frac{1}{\sqrt{2N}} \sum_n e^{i\mathbf{k}(\mathbf{R}_n+\mathbf{t}_{\text{Mo}})} Y_2^{\pm 2}[\mathbf{r} - (\mathbf{R}_n + \mathbf{t}_{\text{Mo}})]$, where

TABLE I. Character table and irreps of the group $\bar{6}m2$ (D_{3h}).

$\bar{6}m2$ (D_{3h})	E	σ_h	$2C_3$	$2S_3$	$3C_2'$	$3\sigma_v$
A_1'	1	1	1	1	1	1
A_2'	1	1	1	1	−1	−1
A_1''	1	−1	1	−1	1	1
A_2''	1	−1	1	−1	−1	−1
E'	2	2	−1	−1	0	0
E''	2	−2	−1	1	0	0

$Y_2^{\pm 2}(\mathbf{r}) \sim [d_{x^2-y^2}(\mathbf{r}) \pm i d_{xy}(\mathbf{r})]/\sqrt{2}$. The small group of the wave vector at the K point is C_{3h}. One can show that $\left|\Psi_{2,2}^{\text{Mo}}(\mathbf{K})\right\rangle$ transforms as the E_2' irrep of this group, whereas $\left|\Psi_{2,-2}^{\text{Mo}}(\mathbf{K})\right\rangle$ transforms as the A' irrep. Since the VB is nondegenerate at the Γ point, compatibility relations require that at the K point it transforms as the A' irrep.

Table I shows the characters and irreps for D_{3h}, pertinent to the Γ point, while Table II shows symmetry properties of the rotating orbitals based Bloch wave functions and that which band they contribute to. The conduction band is denoted by CB, the valence by VB, the first band above the CB by CB $+1$, the first band below the VB by VB-1, and so on.

Table III gives the characters and irreps of C_{3h}, pertinent to the K point and Table IV the rotating orbitals based Bloch wave function which transform as the irreps of C_{3h}.

APPENDIX B: BILAYER GRAPHENE HAMILTONIAN

The $\mathbf{k} \cdot \mathbf{p}$ Hamiltonian of bilayer graphene[35] at the K point of the BZ, in the basis of $\{A2, B1, A1, B2\}$ sites is given by

$$H_{\mathbf{kp}}^{\text{BG}} = \begin{pmatrix} 0 & \gamma_1 & v_4 p_+ & v_0 p_- \\ \gamma_1 & 0 & v_0 p_+ & v_4 p_- \\ v_4 p_- & v_0 p_- & 0 & v_3 p_+ \\ v_0 p_+ & v_4 p_+ & v_3 p_- & 0 \end{pmatrix}, \quad \text{(B1)}$$

where we have chosen the on-site energies to be zero, $p_\pm = p_x \pm i p_y$, the velocities v_0, v_3, and v_4 depend on intra- and interlayer hoppings, and γ_1 is the direct hopping between the atoms $B1$ and $A2$. One can perform a unitary transformation which rotates the Hamiltonian (B1) into the basis $\{|\Psi_{A1}\rangle, |\Psi_{A2}\rangle, |\Psi_{E_1}\rangle, |\Psi_{E_2}\rangle\}$, where the basis functions $|\Psi_\mu\rangle$ transform as the irreps $\mu = \{A1, A2, E\}$ of the small

TABLE II. Basis functions for the irreps of the small group D_{3h} of the Γ point. $\{\cdots\}$ denote the partners of the two-dimensional representations. The rightmost column shows that to which band the basis functions contribute.

irrep	Basis functions	Band
A_1'	$\left|\Psi_{0,0}^{\text{Mo}}\right\rangle, \left|\Psi_{2,0}^{\text{Mo}}\right\rangle, \frac{1}{\sqrt{2}}\left(\left|\Psi_{1,0}^{\text{S1}}\right\rangle - \left|\Psi_{1,0}^{\text{S2}}\right\rangle\right)$	VB
A_2''	$\left|\Psi_{1,0}^{\text{Mo}}\right\rangle, \frac{1}{\sqrt{2}}\left(\left|\Psi_{1,0}^{\text{S1}}\right\rangle - \left|\Psi_{1,0}^{\text{S2}}\right\rangle\right)$	VB-2
E'	$\left\{\left|\Psi_{2,2}^{\text{Mo}}\right\rangle, \left|\Psi_{2,-2}^{\text{Mo}}\right\rangle\right\}$	VB-3
	$\left\{\frac{1}{\sqrt{2}}\left(\left|\Psi_{1,1}^{\text{S1}}\right\rangle - \left|\Psi_{1,1}^{\text{S2}}\right\rangle\right), \frac{1}{\sqrt{2}}\left(\left|\Psi_{1,-1}^{\text{S1}}\right\rangle - \left|\Psi_{1,-1}^{\text{S2}}\right\rangle\right)\right\}$	
E''	$\left\{\left|\Psi_{2,1}^{\text{Mo}}\right\rangle, \left|\Psi_{2,-1}^{\text{Mo}}\right\rangle\right\}$	VB-1
	$\left\{\frac{1}{\sqrt{2}}\left(\left|\Psi_{1,1}^{\text{S1}}\right\rangle - \left|\Psi_{1,1}^{\text{S2}}\right\rangle\right), \frac{1}{\sqrt{2}}\left(\left|\Psi_{1,-1}^{\text{S1}}\right\rangle - \left|\Psi_{1,-1}^{\text{S2}}\right\rangle\right)\right\}$	

TABLE III. Character table of the group $\bar{6}$ (C_{3h}).

$\bar{6}$ (C_{3h})	E	C_3	C_3^2	σ_h	S_3	$\sigma_h C_3^2$
A'	1	1	1	1	1	1
A''	1	1	1	-1	-1	-1
E_1'	1	ω	ω^2	1	ω	ω^2
E_2'	1	ω^2	ω	1	ω^2	ω
E_1''	1	ω	ω^2	-1	$-\omega$	$-\omega^2$
E_2''	1	ω^2	ω	-1	$-\omega^2$	$-\omega$

group of the K point, which is D_3 in this case. One finds

$$H_{\mathbf{kp}}^{\mathrm{BG}} = \begin{pmatrix} -\gamma_1 & 0 & -\tilde{v}_{04}\,p_+ & \tilde{v}_{04}\,p_- \\ 0 & \gamma_1 & \overline{v}_{04}\,p_+ & \overline{v}_{04}\,p_- \\ -\tilde{v}_{04}\,p_- & \overline{v}_{04}\,p_- & 0 & v_3 p_+ \\ \tilde{v}_{04}\,p_+ & \overline{v}_{04}\,p_+ & v_3 p_- & 0 \end{pmatrix}, \quad \text{(B2)}$$

where $\tilde{v}_{04} = \frac{1}{\sqrt{2}}(v_0 - v_4)$, and $\overline{v}_{04} = \frac{1}{\sqrt{2}}(v_0 + v_4)$. This Hamiltonian is characterized by the three hoppings v_3, $\tilde{v}_{04}$, and $\overline{v}_{04}$, and three band-edge energies $-\gamma_1$, γ_1, and 0 (degenerate). The well known low-energy effective Hamiltonian of bilayer graphene[35] can be obtained by projecting out the states $|\Psi_{A1}\rangle$ and $|\Psi_{A2}\rangle$.

The Hamiltonian of monolayer MoS_2 has the same structure as (B2) but is characterized by five different hoppings and four different band-edge energies; in this sense it is a generalization of (B2).

APPENDIX C: Q-POINT MINIMUM IN THE CONDUCTION BAND

In this section we briefly discuss whether it is important to consider the minimum at the Q point in the conduction band (see Fig. 3).

To this end we compare the conduction band calculated in local density approximation (LDA) and using the HSE06 hybrid functional.[45] The latter, while being computationally much more demanding than the LDA, has been shown to improve the accuracy of electronic structure calculations for many semiconductors.[46]

TABLE IV. Basis functions for the irreducible representations of the small group of the K point. The rightmost column shows that to which band the basis functions contribute. The basis functions for the K' point can be obtained by complex conjugation.

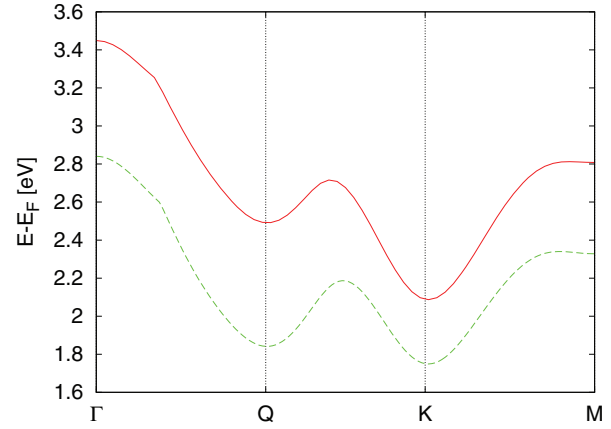| irrep	Basis functions	Band
A'	$\left\|\Psi_{2,-2}^{\mathrm{Mo}}\right\rangle$, $\frac{1}{\sqrt{2}}\left(\left\|\Psi_{1,-1}^{\mathrm{S1}}\right\rangle + \left\|\Psi_{1,-1}^{\mathrm{S2}}\right\rangle\right)$	VB
A''	$\left\|\Psi_{2,1}^{\mathrm{Mo}}\right\rangle$, $\frac{1}{\sqrt{2}}\left(\left\|\Psi_{1,-1}^{\mathrm{S1}}\right\rangle - \left\|\Psi_{1,-1}^{\mathrm{S2}}\right\rangle\right)$	CB + 1
E_1'	$\left\|\Psi_{2,0}^{\mathrm{Mo}}\right\rangle$, $\frac{1}{\sqrt{2}}\left(\left\|\Psi_{1,1}^{\mathrm{S1}}\right\rangle + \left\|\Psi_{1,1}^{\mathrm{S2}}\right\rangle\right)$	CB
E_2'	$\left\|\Psi_{2,2}^{\mathrm{Mo}}\right\rangle$, $\frac{1}{\sqrt{2}}\left(\left\|\Psi_{1,0}^{\mathrm{S1}}\right\rangle - \left\|\Psi_{1,0}^{\mathrm{S2}}\right\rangle\right)$	VB-3
		CB + 2
E_1''	$\left\|\Psi_{1,0}^{\mathrm{Mo}}\right\rangle$, $\frac{1}{\sqrt{2}}\left(\left\|\Psi_{1,1}^{\mathrm{S1}}\right\rangle - \left\|\Psi_{1,1}^{\mathrm{S2}}\right\rangle\right)$	VB-2
E_2''	$\left\|\Psi_{2,-1}^{\mathrm{Mo}}\right\rangle$, $\frac{1}{\sqrt{2}}\left(\left\|\Psi_{1,0}^{\mathrm{S1}}\right\rangle + \left\|\Psi_{1,0}^{\mathrm{S2}}\right\rangle\right)$	VB-1

FIG. 3. (Color online) Conduction band of MoS_2 from DFT calculations using the HSE06 functional (red, solid line) and the LDA (green, dashed line).

As one can see in Fig. 3, there are two main differences between the results of calculated with the HSE06 functional (red, solid line) and LDA (green, dashed line). First, there is an up-shift of the HSE06 conduction band with respect to the LDA one, leading to a larger band gap at K. Second, the minimum at the Q point is much higher in energy (and becomes shallower) than the minimum at K in the case of HSE06 calculations. In particular, the difference between the minima is $E_Q^{\mathrm{hybrid}} - E_K^{\mathrm{hybrid}} = 0.405$ eV for HSE06 and $E_Q^{\mathrm{LDA}} - E_K^{\mathrm{LDA}} = 0.09$ eV for LDA. (Note, that the LDA calculations of Ref. 16 give ≈ 0.2 eV). For comparison, the difference between the valence band maxima are $E_K^{\mathrm{hybrid}} - E_\Gamma^{\mathrm{hybrid}} = 0.058$ eV for HSE06 and $E_K^{\mathrm{LDA}} - E_\Gamma^{\mathrm{LDA}} = 0.12$ eV for LDA. Therefore, regarding transport properties, for p-doped samples states at the Γ point are more important than the states at Q for the n-doped case.

We note that both the increase of the band gap at the K point and the up-shift of the minimum at the Q point are in qualitative agreement with the GW calculations of Ref. 17. The importance of the Q point minimum can hopefully be determined when more accurate measurements of mobility become available, because the phonon-limited mobility depends quite sensitively on the energy separation of $E_K - E_Q$ (for details see Refs. 16 and 25).

By contrast, the energy difference between the top of the valence band at the Γ and K points shows much smaller dependence on the choice of the computational method.

TABLE V. Parameters of the effective Hamiltonian. m_e is the bare electron mass.

	LDA	HSE06
α	1.73 eV Å^2	1.57 eV Å^2
β	-0.13 eV Å^2	0.1 eV Å^2
γ_3	3.82 eV Å	4.13 eV Å
κ	-1.02 eV Å^2	-1.12 eV Å^2
η	8.53 eV Å^3	7.87 eV Å^3
m_{eff}^c/m_e	0.48	0.43
m_{eff}^v/m_e	-0.62	-0.53
$m_{\mathrm{eff}}^\Gamma/m_e$	-3.65	-2.24

APPENDIX D: k · p PARAMETERS FROM CALCULATIONS WITH HSE06 HYBRID FUNCTIONAL

Comparison between experimental data and DFT calculations suggest[47] that in the case of semiconductors hybrid functionals[45] not only produce band gaps which are in better agreement with measurements but also the calculated effective masses are closer to the experimental values. Motivated by this we have also fitted our model to LDA band structure calculations performed with the HSE06 functional.[48] The main effect at the K point seems to be that the effective masses become lighter and the coupling parameter γ_3 stronger. However, the change in the effective mass at the Γ point is more significant. In Table V we show the relevant band parameters calculated both with LDA and using HSE06.

*andor.kormanyos@uni-konstanz.de

[1] Q. H. Wang, K. Kalantar-Zadeh, A. Kis, J. N. Coleman, and M. S. Strano, Nat. Nanotechnol. **7**, 699 (2012).

[2] B. Radisavljević, A. Radenović, J. Brivio, V. Giacometti, and A. Kis, Nat. Nanotechnol. **6**, 147 (2011).

[3] A. Splendiani, L. Sun, Y. Zhang, T. Li, J. Kim, Ch.-Y. Chim, G. Galli, and F. Wang, Nano Lett. **10**, 1271 (2010).

[4] G. Eda, H. Yamaguchi, D. Voiry, T. Fujita, M. Chen, and M. Chhowalla, Nano Lett. **11**, 5111 (2011).

[5] H. Zeng, J. Dai, W. Yao, D. Xiao, and X. Cui, Nat. Nanotechnol. **7**, 490 (2012).

[6] K. F. Mak, K. He, J. Shan, and T. F. Heinz, Nat. Nanotechnol. **7**, 494 (2012).

[7] T. Cao, G. Wang, W. Han, H. Ye, Ch. Zhu, J. Shi, Q. Niu, P. Tan, E. Wang, B. Liu, and J. Feng, Nat. Commun. **3**, 887 (2012).

[8] S. Wu, J. S. Ross, G.-B. Liu, G. Aivazian, A. Jones, Z. Fei, W. Zhu, D. Xiao, W. Yao, D. Cobden, and X. Xu, Nature Physics **9**, 149 (2013).

[9] G. Sallen, L. Bouet, X. Marie, G. Wang, C. R. Zhu, W. P. Han, Y. Lu, P. H. Tan, T. Amand, B. L. Liu, and B. Urbaszek, Phys. Rev. B **86**, 081301 (2012).

[10] M. Buscema, M. Barkelid, V. Zwiller, H. S. J. van der Zant, G. A. Steele, and A. Castellanos-Gomez, Nano Lett. **13**, 358 (2013).

[11] A. M. Jones, H. Yu, N. Ghimire, S. Wu, G. Aivazian, J. S. Ross, B. Zhao, J. Yan, D. Mandrus, D. Xiao, W. Yao, and X. Xu, arXiv:1303.5318.

[12] D. Xiao, G.-B. Liu, W. Feng, X. Xu, and W. Yao, Phys. Rev. Lett. **108**, 196802 (2012).

[13] H.-Zh. Lu, W. Yao, D. Xiao, and Sh.-Q. Shen, Phys. Rev. Lett. **110**, 016806 (2013).

[14] X. Li, F. Zhang, and Q. Niu, Phys. Rev. Lett. **110**, 066803 (2013).

[15] Z. Y. Zhu, Y. C. Cheng, and U. Schwingenschlögl, Phys. Rev. B **84**, 153402 (2011).

[16] K. Kaasbjerg, K. S. Thygesen, and K. W. Jacobsen, Phys. Rev. B **85**, 115317 (2012).

[17] T. Cheiwchanchamnangij and W. R. L. Lambrecht, Phys. Rev. B **85**, 205302 (2012).

[18] A. Ramasubramaniam, Phys. Rev. B **86**, 115409 (2012).

[19] K. Kośmider and J. Fernández-Rossier, Phys. Rev. B **87**, 075451 (2013).

[20] H. Shi, H. Pan, Y.-W. Zhang, and B. I. Yakobson, Phys. Rev. B **87**, 155304 (2013).

[21] J. K. Ellis, M. J. Lucero, and G. E. Scuseria, Appl. Phys. Lett. **99**, 261908 (2011).

[22] E. S. Kadantsev and P. Hawrylak, Solid State Commun. **152**, 909 (2012).

[23] W. S. Yun, S. W. Han, S. Ch. Hong, I. G. Kim, and J. D. Lee, Phys. Rev. B **85**, 033305 (2012).

[24] W. Feng, Y. Yao, W. Zhu, J. Zhou, W. Yao, and D. Xiao, Phys. Rev. B **86**, 165108 (2012).

[25] X. Li, J. T. Mullen, Zh. Jin, K. M. Borysenko, M. Buongiorno Nardelli, and K. W. Kim, Phys. Rev. B **87**, 115418 (2013).

[26] K. Dolui, I. Rungger, and S. Sanvito, Phys. Rev. B **87**, 165402 (2013).

[27] R. Roldán, E. Cappelluti, and F. Guinea, arXiv:1301.4836.

[28] Y. Song and H. Dery, arXiv:1302.3627 [Phys. Rev. Lett. (to be published)].

[29] H. Ochoa and R. Roldán, Phys. Rev. B **87**, 245421 (2013).

[30] R. A. Bromley, R. B. Murray, and A. D. Yoffe, J. Phys. C: Solid State Phys. **5**, 759 (1972).

[31] L. F. Mattheis, Phys. Rev. B **8**, 3719 (1973).

[32] M. S. Dresselhaus, G. Dresselhaus, and A. Jorio, *Group Theory* (Springer, Berlin, 2008).

[33] S. Konschuh, M. Gmitra, D. Kochan, and J. Fabian, Phys. Rev. B **85**, 115423 (2012).

[34] A. Kormányos and G. Burkard, Phys. Rev. B **87**, 045419 (2013).

[35] E. McCann and V. I. Fal'ko, Phys. Rev. Lett. **96**, 086805 (2006).

[36] R. Winkler, *Spin-Orbit Coupling Effects in Two-Dimensional Electron and Hole Systems* (Springer, Berlin, 2003).

[37] G. Kresse and J. Furthmüller, Phys. Rev. B **54**, 11169 (1996).

[38] The plane-wave cutoff energy was 600 eV. We used a 12×12 Monkhorst-Pack k-point grid in the 2D plane to relax the structure and a 24×24 grid to calculate the band structure. The optimized lattice parameter was 3.129 Å and the distance between the two layers of S atoms was 3.114 Å.

[39] Ch.-X. Liu, X.-L. Qi, H. J. Zhang, X. Dai, Zh. Fang, and Sh.-Ch. Zhang, Phys. Rev. B **82**, 045122 (2010).

[40] The matrix elements of the momentum operator were evaluated within the LDA using the CASTEP code,[41] because the necessary plane-wave coefficients of the wave functions at the band edges were readily accessible in the output of CASTEP. We used norm-conserving pseudopotentials, a plane-wave cutoff energy of 80 Ha, an artificial periodicity of 30 Bohr in the vertical direction, and a 21×21 Monkhorst-Pack mesh. The optimized lattice parameter and the S-S distance was the same as in the case of VASP calculations, see Ref. 38.

[41] S. J. Clark *et al.*, Z. Kristallogr. **220**, 567 (2005).

[42] The SOC in the conduction band was briefly mentioned in Ref. 29 and noted that its value is, in principle, nonzero, but no detailed discussion was given.

[43]T. S. Jespersen, K. G. Rasmussen, J. Paaske, K. Muraki, T. Fujisawa, J. Nygård, and K. Flensberg, Nat. Phys. **7**, 348 (2011).

[44]H. Rostami, A. G. Moghaddam, and R. Asgari, arXiv: 1302.5901.

[45]J. Heyd, G. E. Scuseria, and M. Ernzerhof, J. Chem. Phys. **118**, 8207 (2003); **124**, 219906 (2006).

[46]B. G. Janesko, T. M. Henderson, and G. E. Scuseria, PhysChemChemPhys **11**, 443 (2009).

[47]Y.-S. Kim, M. Marsman, G. Kresse, F. Tran, and P. Blaha, Phys. Rev. B **82**, 205212 (2010).

[48]The plane-wave cutoff energy was 600 eV and we used 24×24 Monkhorst-Pack k-point grid to calculate the band structure.